J. Plasma Physics (2014), *vol.* 80, *part* 4, *pp.* 531–551.
doi:10.1017/S0022377814000154

Phase space scales of free energy dissipation in gradient-driven gyrokinetic turbulence

D. R. Hatch[1,2,†], F. Jenko[2,3], V. Bratanov[2] and A. Bañón Navarro[2]

[1]Institute for Fusion Studies, University of Texas at Austin, Austin, TX 78712, USA
[2]Max-Planck-Institut für Plasmaphysik, Boltzmannstr. 2, D-85748 Garching, Germany
[3]Max-Planck/Princeton Center for Plasma Physics

(Received 20 December 2013; revised 25 February 2014; accepted 10 March 2014; first published online 6 May 2014)

A reduced four-dimensional (integrated over perpendicular velocity) gyrokinetic model of slab ion temperature gradient-driven turbulence is used to study the phase-space scales of free energy dissipation in a turbulent kinetic system over a broad range of background gradients and collision frequencies. Parallel velocity is expressed in terms of Hermite polynomials, allowing for a detailed study of the scales of free energy dynamics over the four-dimensional phase space. A fully spectral code – the DNA code – that solves this system is described. Hermite free energy spectra are significantly steeper than would be expected linearly, causing collisional dissipation to peak at large scales in velocity space even for arbitrarily small collisionality. A key cause of the steep Hermite spectra is a *critical balance* – an equilibration of the parallel streaming time and the nonlinear correlation time – that extends to high Hermite number n. Although dissipation always peaks at large scales in all phase space dimensions, small-scale dissipation becomes important in an integrated sense when collisionality is low enough and/or nonlinear energy transfer is strong enough. Toroidal full-gyrokinetic simulations using the GENE code are used to verify results from the reduced model. Collision frequencies typically found in present-day experiments correspond to turbulence regimes slightly favoring large-scale dissipation, while turbulence in low-collisionality systems like ITER and space and astrophysical plasmas is expected to rely increasingly on small-scale dissipation mechanisms. This work is expected to inform gyrokinetic reduced modeling efforts like Large Eddy Simulation and gyrofluid techniques.

1. Introduction

The most fundamental turbulence paradigm is that of the Kolmogorov cascade and the associated drive and dissipation ranges in three-dimensional, homogeneous, high-Reynolds-number Navier–Stokes turbulence: energy is injected at large scales, cascades conservatively through a broad inertial range, and is dissipated at small scales where viscous dissipation becomes comparable to inertial forces. Despite several decades of study (Krommes 2012) and a continually-broadening area of application (from magnetic confinement fusion (Doyle et al. 2007; Garbet et al. 2010) to space and astrophysics (Howes et al. 2006; Schekochihin et al. 2009; Howes et al. 2011a; Pueschel et al. 2011; TenBarge and Howes 2012), a comparable coherent overall picture is still developing in gyrokinetic turbulence. Certain aspects of the fluid picture carry over

† Email address for correspondence: drhatch@austin.utexas.edu

to gyrokinetics; cascade dynamics have been identified (Navarro et al. 2011b; Plunk and Tatsuno 2011; Teaca et al. 2012) and power laws have been derived in simplified and idealized cases (Plunk et al. 2010; Barnes et al. 2011), although these spectra are not universal and can be modified by linear drive and/or dissipation (Görler and Jenko 2008; Cerri 2013). The final piece of turbulent energy balance – dissipation – is largely decoupled from the aforementioned power laws, and differs strikingly from the fluid picture; in gyrokinetic systems dissipation can peak at large scales, and there appears to be little scale separation between drive and dissipation (Hatch et al. 2011b; Navarro et al. 2011a, b; Teaca et al. 2012).

This question of the scales and parameter dependences of dissipation in gyrokinetic systems remains largely un-addressed and is the focus of this work. The topic is important not only in the context of fundamental turbulence studies, but also to ensure accurate prediction of transport quantities in fusion devices with reasonable computational resources. A fundamental understanding of dissipation in gyrokinetic systems is expected to facilitate and inform reduced-modeling techniques like Large Eddy Simulations (Navarro et al. 2014) and gyrofluid approximations (Dorland and Hammett 1993).

Dissipation in gyrokinetics is due to collisions, which, in comparison with viscous dissipation in neutral fluid systems, is also described by a (largely) diffusive operator, albeit in velocity space rather than real space. As such, the gyrokinetic energy sink is enhanced by small scales in velocity space, but not directly tied to small scales in real space. Nonetheless, real space scales are indirectly connected to velocity space scales in the context of the two main mechanisms responsible for development of velocity space structure in gyrokinetic systems – linear phase mixing (Landau damping) and nonlinear perpendicular phase mixing. The former is a linear phenomenon connected with parallel (to the magnetic field) scales in both real and velocity space (Landau 1946; Hammett et al. 1992; Watanabe and Sugama 2006). Nonlinear phase mixing is a nonlinear process that is intrinsically small scale (active at $k_\perp \rho_i > 1$, where $k_\perp$ is the wavenumber in a direction perpendicular to the magnetic field and ρ_i is the ion gyroradius) and links small-scale structures in perpendicular velocity space and real space (Schekochihin et al. 2008; Tatsuno et al. 2009; Plunk et al. 2010).

Dissipation has been observed to peak at large perpendicular spatial scales in gyrokinetic simulations, and a large portion of the energy can be dissipated at scales where nonlinear phase mixing is not active. This large-scale dissipation has been interpreted using the damped eigenmode paradigm (Terry et al. 2006; Hatch et al. 2011b, c; Makwana et al. 2014) – nonlinear excitation of linearly stable modes at scales comparable to those of the driving instabilities. In gyrokinetics, these damped modes are characterized by progressively smaller scales in parallel real space and velocity space (Hatch et al. 2011b), suggesting a link with linear phase mixing – i.e. nonlinear excitation of Landau-damped modes at large perpendicular scales. In this work, we focus directly on the linear phase mixing mechanism in the context of ion temperature gradient (ITG) driven turbulence with the goal of systematically elucidating the role and importance of large and small scales in phase space with regard to free energy dissipation. To this end we study a reduced-gyrokinetic system in order to clearly identify the phase space (velocity and real space) scales at which dissipation occurs. We find that collisional dissipation peaks at large scales in *all* phase space dimensions, and spreads to small scales as collisionality decreases and/or nonlinear energy transfer increases. The collision-frequencies characterizing present-day fusion devices represent turbulent scenarios where dissipation slightly favors large scales ($k_\perp \rho_i < 1$). In other less-collisional scenarios (e.g. ITER-motivated parameter

regimes and many space and astrophysical systems), dissipation is expected to occur predominantly at small scales ($k_\perp \rho_i > 1$), and nonlinear phase mixing is expected to be an increasingly important dissipation mechanism.

This paper builds on (Hatch et al. 2013) and augments the material therein by examining several key points in more detail and presenting a campaign of full-gyrokinetic simulations using the GENE code (Jenko et al. 2000) that verifies and expands on many of the results achieved using the reduced model. The paper is outlined as follows: In Sec. 2, we describe the simplified gyrokinetic model used in this work, and the associated free energy evolution equation. Hermite polynomials are used to represent parallel velocity space, providing a useful basis for studying energy transfer and dissipation in phase space scales. In Sec. 3 we introduce the DNA code – a fully spectral code created to solve the system of equations described in Sec. 2 – and describe the numerical implementation of the simulations. In Sec. 4 we examine the Hermite free energy spectrum and derive an expression for the scaling of the spectrum as a function of various dissipation parameters. A key step in this process is the identification of a critical balance (Goldreich and Sridhar 1995; Barnes et al. 2011; TenBarge and Howes 2012) – between the nonlinear correlation time and the characteristic parallel streaming time – that extends to high n in Hermite space, where n is the Hermite number. This critical balance is examined in detail in Sec. 4, along with numerical verification of the predicted Hermite spectra. The main conclusion here is that the Hermite spectrum is steepened nonlinearly to the extent that collisional dissipation peaks at large scales in velocity space. In Sec. 5, the insight gained in Sec. 4 is applied to an examination and interpretation of the dissipation scales in the full four-dimensional phase space. Dissipation is shown to peak at large scales in phase space and spread to progressively smaller scales as collisionality decreases and/or nonlinear energy transfer increases. Section 6 presents complementary toroidal full-gyrokinetic simulations scanning the collision frequency and temperature gradient scale length using the GENE code. A summary and discussion are provided in Sec. 7.

2. Model

2.1. *Fourier–Hermite representation*

The model used in this work is chosen to be as simple as possible while still rigorously describing the dynamics of interest. We study ITG-driven turbulence in an unsheared slab in the context of a simplified nonlinear gyrokinetic system. The simplification entails an integration of the gyrokinetic equations over the perpendicular velocity $v_\perp$, replacing gyroaverage operators with factors of $e^{-k_\perp^2/2}$. This treatment is exact when integrating over a Maxwellian (in $v_\perp$) distribution function, as is done for all gyroaverages of the electrostatic potential. The use of this simplified gyroaverage operator on the perturbed distribution function in the Poisson equation (3) is an approximation that is well justified for scales larger than $k_\perp \rho_i \sim 1$ (Dorland and Hammett 1993). In the numerical results described below, simulations are limited to these scales. By doing this we intentionally neglect nonlinear phase mixing (which becomes important at $k_\perp \rho_i > 1$) and model small-scale dissipative processes using $k_\perp$ hyperdiffusion. We roughly interpret dissipation due to this hyperdiffusion term as an upper bound on the dissipation that would be attributable to nonlinear phase mixing in a more comprehensive system. The model is similar to the model described in (Watanabe and Sugama 2004) except that we retain a full range of scales in the parallel direction.

The transparency of the model is further enhanced by employing a Hermite decomposition in parallel velocity space,

$$f(v) = \sum_{n=0}^{\infty} \hat{f}_n H_n(v) e^{-v^2}, \tag{1}$$

where $H_n(x) = (n!\,2^n \pi^{1/2})^{-1/2} e^{x^2}(-d/dx)^n e^{-x^2}$ (several examples of the basis functions are shown in Fig. 2). Hermite polynomials have a substantial history in the context of representing velocity space scales in a variety of kinetic plasma systems (Grant and Feix 1967; Armstrong et al. 1970; Hammett et al. 1993; Watanabe and Sugama 2004; Zocco and Schekochihin 2011). They have recently been shown to optimally represent velocity space in gyrokinetic simulations (Hatch et al. 2012) and to facilitate accurate solutions of linear kinetic operators (Bratanov et al. 2013). The normalized reduced gyrokinetic equation in the Hermite basis reads

$$\begin{aligned}\frac{\partial \hat{f}_{\mathbf{k},n}}{\partial t} = {} & \frac{\eta_i i k_y}{\pi^{1/4}} \frac{k_\perp^2}{2} \bar{\phi}_{\mathbf{k}} \delta_{n,0} - \frac{i k_y}{\pi^{1/4}} \bar{\phi}_{\mathbf{k}} \delta_{n,0} - \frac{\eta_i i k_y}{2^{1/2} \pi^{1/4}} \bar{\phi}_{\mathbf{k}} \delta_{n,2} \\ & - \frac{i k_z}{\pi^{1/4}} \bar{\phi}_{\mathbf{k}} \delta_{n,1} - i k_z \left(\sqrt{n}\, \hat{f}_{\mathbf{k},n-1} + \sqrt{n+1}\, \hat{f}_{\mathbf{k},n+1} \right) \\ & - \nu n \hat{f}_{\mathbf{k},n} + \sum_{\mathbf{k}'} \left(k_x' k_y - k_x k_y' \right) \bar{\phi}_{\mathbf{k}'} \hat{f}_{\mathbf{k}-\mathbf{k}',n}, \end{aligned} \tag{2}$$

where $\hat{f}_{\mathbf{k},n}(\rho_i n_{i0}/L_n v_{ti}^3)$ is the ion distribution function, n_{i0} is the ion density, L_n is the density gradient scale length, v_{ti} is the ion thermal velocity, n denotes the order of the Hermite polynomial, $t(L_n/v_{ti})$ is time, η_i is the ratio of L_n to the temperature gradient scale length L_T, $k_y(\rho_i^{-1})$ is the Fourier wavenumber for the direction perpendicular to both the direction of the background gradients $[x \rightarrow k_x(\rho_i^{-1})]$ and the coordinate aligned with the magnetic field $[z \rightarrow k_z(L_n^{-1})]$. The perpendicular wavenumber is $k_\perp = (k_x^2 + k_y^2)^{1/2}$, $\bar{\phi}_{\mathbf{k}}(\rho_i T_{e0}/L_n e)$ is the gyro-averaged electrostatic potential, T_{e0} is the background electron temperature, e is the elementary charge, and $\nu(v_{ti}/L_n)$ is the collision frequency. We use the Lenard–Bernstein collision operator (Lenard and Bernstein 1958) for the parallel velocity, for which Hermite polynomials are eigenvectors: $\nu\partial_v[(1/2)\partial_v + v] \rightarrow \nu n$. The electrostatic potential is directly proportional to the zeroth-order Hermite polynomial as determined by

$$\phi_{\mathbf{k}} = \pi^{1/4} e^{-k_\perp^2/2} \hat{f}_{\mathbf{k},0} / [\tau + 1 - \Gamma_0(k_\perp^2)], \tag{3}$$

where τ is the ratio of the ion to electron temperature, and $\Gamma_0(x) = e^{-x} I_0(x)$, with I_0 the zeroth-order modified Bessel function. Note that here we do not remove the flux-surface-averaged potential, as this treatment strongly suppresses the turbulence in slab simulations (Watanabe and Sugama 2004).

To substantiate the expectation that we capture the salient dynamics with this reduced model, we verify and expand on the main results regarding $k_\perp$ dissipation scales with high resolution, toroidal, full-gyrokinetic simulations using the GENE code, as described in Sec. 6.

2.2. *Free energy conservation and evolution*

The free energy

$$\varepsilon_{\mathbf{k},n} = \varepsilon_{\mathbf{k}}^{(\phi)} \delta_{n,0} + \varepsilon_{\mathbf{k},n}^{(f)}, \tag{4}$$

with electrostatic component

$$\varepsilon_{\mathbf{k}}^{(\phi)} = \frac{1}{2}(\tau + 1 - \Gamma_0(k_\perp^2))^{-1}|\phi_{\mathbf{k}}|^2 \tag{5}$$

and entropy component

$$\varepsilon_{\mathbf{k},n}^{(f)} = \frac{1}{2}\pi^{1/2}|\hat{f}_{\mathbf{k},n}|^2 \tag{6}$$

is the ideal quadratic invariant in gyrokinetics, and plays a role analogous to kinetic energy in neutral fluid turbulence (Navarro et al. 2011a; Plunk et al. 2012). The **k**- and n-resolved free energy evolution equation is readily derived with the help of (2) and (3). One thus obtains

$$\frac{\partial \varepsilon_{\mathbf{k},n}^{(\phi)}}{\partial t} = J_{\mathbf{k}}^{(\phi)}\delta_{n,0} + N_{\mathbf{k},n}^{(\phi)} \tag{7}$$

and

$$\frac{\partial \varepsilon_{\mathbf{k},n}^{(f)}}{\partial t} = \eta_i Q_{\mathbf{k}}\delta_{n,2} - C_{\mathbf{k},n} - J_{\mathbf{k}}^{(\phi)}\delta_{n,1} + J_{\mathbf{k},n-1/2} - J_{\mathbf{k},n+1/2} + N_{\mathbf{k},n}^{(f)}. \tag{8}$$

The terms on the RHS of (7) and (8) represent various energy injection, dissipation, and transfer channels, and are schematically represented in Fig. 1. The energy source $\eta_i Q_{\mathbf{k}} = \eta_i \Re[-\frac{\pi^{1/4}}{2^{1/2}} i k_y \hat{f}_2^* \bar{\phi}]$ is proportional to the radial ion heat flux $Q_{\mathbf{k}}$ and limited to $n = 2$ as represented by the red arrow in Fig. 1. The energy sink – collisional dissipation $C_{\mathbf{k},n} = 2\nu n \varepsilon_{\mathbf{k},n}^{(f)}$ – is directly proportional to the Hermite number n multiplied by the free energy, and is shown by the blue arrows in Fig. 1. There are also two conservative energy transfer channels. The nonlinear energy transfer $N_{\mathbf{k},n}^{(f)}$ (yellow curved arrows) redistributes energy in k space but does not transfer energy between different n. The linear phase mixing terms $J_{\mathbf{k},n-1/2} = \Re[-\pi^{1/2} i k_z \sqrt{n}\hat{f}_{\mathbf{k},n}^* \hat{f}_{\mathbf{k},n-1}]$ and $J_{\mathbf{k},n+1/2} = \Re[\pi^{1/2} i k_z \sqrt{n+1}\hat{f}_{\mathbf{k},n}^* \hat{f}_{\mathbf{k},n+1}]$ represent energy transfer between n and $n-1$, $n+1$ respectively, as denoted by the vertical yellow arrows in Fig. 1. The notation $J_{n\pm1/2}$ used for the phase mixing terms reflects the conservative nature of the energy transfer: the energy transferred from n_0 to n_0+1 ($-J_{\mathbf{k},n_0+1/2} = -\Re[\pi^{1/2} i k_z \sqrt{n_0+1}\hat{f}_{\mathbf{k},n_0}^* \hat{f}_{\mathbf{k},n_0+1}]$) is equal to the energy received by n_0+1 from n_0 ($J_{\mathbf{k},(n_0+1)-1/2} = \Re[-\pi^{1/2} i k_z \sqrt{n_0+1}\hat{f}_{\mathbf{k},n_0+1}^* \hat{f}_{\mathbf{k},n_0}]$). This elucidates the role of these phase mixing terms as a linear and completely local transfer mechanism in Hermite space. $J_{\mathbf{k}}^{(\phi)} = \Re[-i k_z \phi^{1/4} \bar{\phi}^* \hat{f}_{\mathbf{k},1}]$ is the energy transferred between the electrostatic component at $n = 0$ and the entropy component (i.e. Landau damping), represented by the diagonal yellow arrow in Fig. 1. The **k**- and n-summed energy equation reduces to a balance of the net energy sources $\eta_i Q$ and sinks C. The scales in the full phase space at which this balance is achieved depend on the interplay between the dissipation and the conservative energy transfer channels, and will be examined in detail below.

3. DNA code and simulations

A fully spectral code has been created to solve (2) and (3). The code is named the DNA code due to several algorithmic and structural influences from the gyrokinetic GENE code. The code uses a Fourier representation in the three spatial dimensions and a Hermite basis in parallel velocity space. An explicit fourth-order Runge-Kutta (RK4) time scheme is used, with an initial time step constrained to keep the most extreme

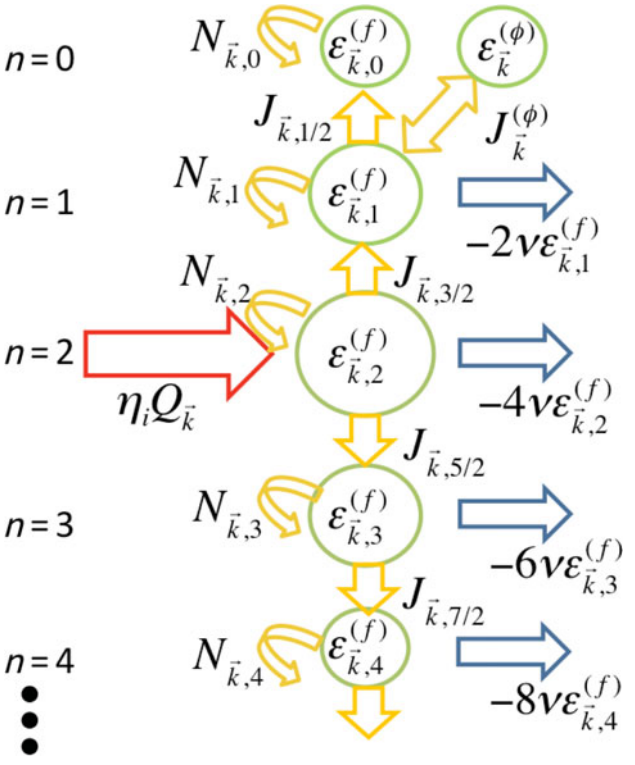

FIGURE 1. A schematic representation of the n- and $\mathbf{k}$-resolved free energy evolution [quantified in (8)]. Energy is injected at $n = 2$ (red arrow), conservatively redistributed in k space via nonlinear energy transfer (yellow curved arrows), conservatively transferred in n space by linear phase mixing (yellow vertical arrows), and dissipated by collisional dissipation (blue arrows).

stable eigenvalues within the RK4 stability boundary. The time step is thereafter dynamically adapted in the nonlinear regime to satisfy a Courant-Friedrichs-Lewy (CFL) criterion relating the resolved perpendicular spatial scales to the fastest $E \times B$ drift velocity in the simulation. Parallelization is implemented in Hermite space using message passing interface (MPI); the code scales efficiently up to $n_{\max}/2$ processors where $n_{\max}$ is the number of Hermite polynomials used in the simulation.

The number of Hermite polynomials used in a simulation must be chosen in conjunction with the collision frequency in order to eliminate artificial effects due to truncation in Hermite space. A simple zero boundary condition (i.e. setting $\hat{f}_{n_{\max}+1} = 0$) is sufficient if enough Hermite polynomials are kept. However, efficiency can be improved by applying hypercollisions (Loureiro et al. 2013) $\nu_h(n/n_{max})^p$ in addition to the physical collision operator νn (here we use eighth-order hypercollisions). This treatment retains the effects of the physical collision operator throughout n space while reducing the necessary resolution by cutting off the tail of the Hermite spectrum more sharply. The truncation is further improved by applying the boundary condition (Loureiro et al. 2013) $\hat{f}_{n_{\max}+1} = ik_z\sqrt{n_{\max}+1}\hat{f}_n/(\nu_h)(n_{\max}+1/n_{\max})^8$.

We use a box size of $125.7\rho_i$ (increased to 144.4 in some simulations) in the x and y directions, and resolve up to $k_{x,y}^{(\max)} = 1.55$. Hyperdiffusion (Barnes et al. 2011) of the form $\nu_\perp(k_{x,y}/k_{x,y}^{(\max)})^8\hat{f}_{\mathbf{k},n}$ is employed in the perpendicular spatial directions in order to cut off the spectrum at $k_\perp\rho_i \sim 1.0$ while leaving the scales $k_\perp\rho_i < 1$

virtually unaffected. The simulations saturate even without the hyperdiffusion, albeit with artificially flat free energy spectra in $k_\perp$ due to accumulation of energy at the $k_{\perp\max}$ boundary. The coefficient $\nu_\perp$ is tuned so that spectral indices of $\sim -7/3$ are maintained for the k_x and k_y free energy spectra between the outer scale and $k_\perp \sim 1.0$. For the parallel direction, the box size is $62.8L_n$, and the simulations resolve up to $k_z = 4.7$. In the literature, $k = 0$ modes are often artificially deleted (Parker et al. 1994; Watanabe and Sugama 2004) for slab ITG simulations. We opt to dynamically evolve all $k = 0$ modes and implement a Krook damping term for $k_z = 0$ and $k_z = k_z^{(\min)}$ modes in order to avoid slowly growing low-k_z modes that fail to saturate (this is only necessary at very low collisionality and/or high gradient drive). This Krook term is always a small fraction of the total dissipation.

4. Critical balance and Hermite spectra

4.1. *High n energy equations*

We first wish to identify the scaling of the Hermite free energy spectrum, which directly determines the dissipation scales in velocity space and, by extension, in k space. To this end we study the steady-state $n \gg 1$ free energy equation (Watanabe and Sugama 2004; Zocco and Schekochihin 2011)

$$|k_z| \frac{\partial}{\partial n} \sqrt{n} \varepsilon_{\mathbf{k},n} = \frac{1}{2} N^{(f)}_{\mathbf{k},n} - \nu n \varepsilon_{\mathbf{k},n}. \tag{9}$$

See Appendix for a discussion of this equation, which is an approximation of (8); numerical tests indicate that this approximation does introduce significant deviations from the exact energy equation but nevertheless preserves enough fidelity to accurately predict the n dependence of the free energy.

It is useful to consider k_z- and $\mathbf{k}$-summed versions of (9):

$$\frac{\partial}{\partial n} \langle k_z \rangle_{\mathbf{k}_\perp,n} \sqrt{n} \varepsilon_{\mathbf{k}_\perp,n} = N^{(f)}_{\mathbf{k}_\perp,n} - \nu n \varepsilon_{\mathbf{k}_\perp,n} \tag{10}$$

and

$$\frac{\partial}{\partial n} \langle k_z \rangle_n \sqrt{n} \varepsilon_n = -\nu n \varepsilon_n, \tag{11}$$

where $\varepsilon_n = \sum_{\mathbf{k}} \varepsilon_{\mathbf{k},n}$ and

$$\langle k_z \rangle_n = \frac{\sum_{\mathbf{k}} |k_z| \varepsilon^{(f)}_{\mathbf{k},n}}{\sum_{\mathbf{k}} \varepsilon^{(f)}_{\mathbf{k},n}}. \tag{12}$$

The terms $\varepsilon_{\mathbf{k}_\perp,n}$ and $\langle k_z \rangle_{\mathbf{k}_\perp,n}$ are defined analogously with the $\mathbf{k}$ sums being replaced by k_z sums.

Equation (11) can be solved in the case of fixed (no n dependence) $\langle k_z \rangle_n$ (Watanabe and Sugama 2004; Zocco and Schekochihin 2011), resulting in a $n^{-1/2}$ scaling for the Hermite free energy spectrum. In the model used in this work, the characteristic parallel wavenumber is free to adjust self-consistently to the turbulent dynamics and is therefore key for determining the scaling of the Hermite free energy spectrum. In the next subsection we show that critical balance sets the characteristic parallel wavenumber $\langle k_z \rangle_n$ in such a way that the Hermite spectra are much steeper than would otherwise be expected.

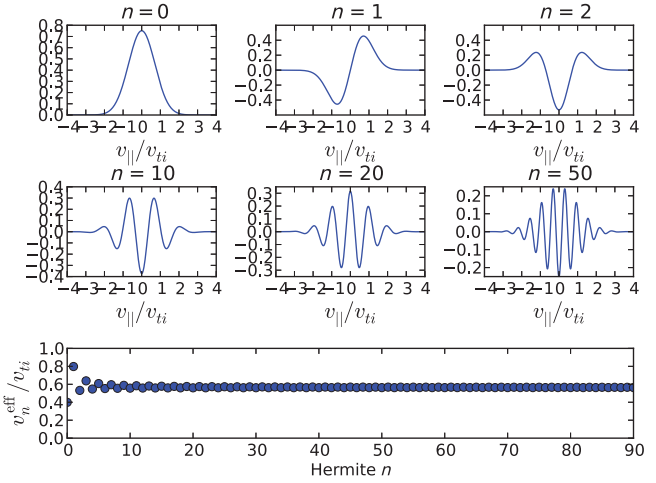

FIGURE 2. (Colour online) Examples of several Hermite basis functions. Note that the thermal velocity v_{ti} sets the envelope of each basis function even as the basis functions are characterized by increasingly small-scale structure in velocity space. This is quantified in the bottom panel, where the characteristic parallel velocity defined by $v_n^{\rm eff}/v_{ti} = \int |v|(H_n(v)e^{-v^2})^2 dv / \int (H_n(v)e^{-v^2})^2 dv$ is plotted. $v_n^{\rm eff}/v_{ti}$ asymptotes to a constant value as n increases.

4.2. *Critical balance*

Critical balance – an equilibration between the nonlinear decorrelation time and the linear parallel wave propagation time – has typically been applied to low-order moments – to magnetic fluctuations in the context of magnetohydrodynamics (MHD) (Goldreich and Sridhar 1995) and kinetic Alfven wave turbulence (TenBarge and Howes 2012), and to the electrostatic potential in ITG-driven systems (Barnes et al. 2011). Here we apply critical balance to moments of arbitrary order by extending the concept to high n in Hermite space. As in (Barnes et al. 2011), we take the characteristic parallel velocity to be the thermal velocity v_{ti}. Due to the Maxwellian weighting in the Hermite basis functions [see (1)], the thermal velocity continues to define the envelope of the basis functions as n increases and the basis functions develop fine scale structure. This is demonstrated quantitatively in the bottom panel of Fig. 2, where the characteristic velocity $v_n^{\rm eff}/v_{ti} = \int |v|(H_n(v)e^{-v^2})^2 dv / \int (H_n(v)e^{-v^2})^2 dv$ is plotted; the characteristic velocity fluctuates at low n (it is enhanced for odd n) and asymptotes to a constant at higher n.

Having established the thermal velocity as a characteristic velocity for all n, the parallel streaming time is $(\langle k_z \rangle_n v_{ti})^{-1}$, which, when normalized to L_n/v_{ti}, is simply the inverse of the normalized characteristic parallel wavenumber $\langle k_z \rangle_n$ defined above in (12). In order to examine critical balance and the resulting Hermite spectra, we study a series of collisionless (retaining only $k_\perp$ hyperdiffusion and hypercollisions) simulations scanning the driving gradient $\eta_i = [5.0, 7.5, 10.0]$. Critical balance is established by comparing the parallel streaming time to the nonlinear correlation function $R_{k_\perp,n}(\tau) = \Re[\int \hat{f}^*_{k_\perp,n}(t+\tau)\hat{f}_{k_\perp,n}(t)dt / \int |\hat{f}_{k_\perp,n}|^2 dt]$, where $\hat{f}_{k_\perp,n} = \sum_{k_z} \hat{f}_{\mathbf{k},n}$. This comparison is shown in Fig. 3, where n-resolved temporal correlation functions for several representative wavenumbers are shown along with the corresponding characteristic parallel streaming times. Critical balance is verified by the striking degree to which the parallel streaming time tracks the contours of the nonlinear correlation time, even reproducing the fluctuations at low n.

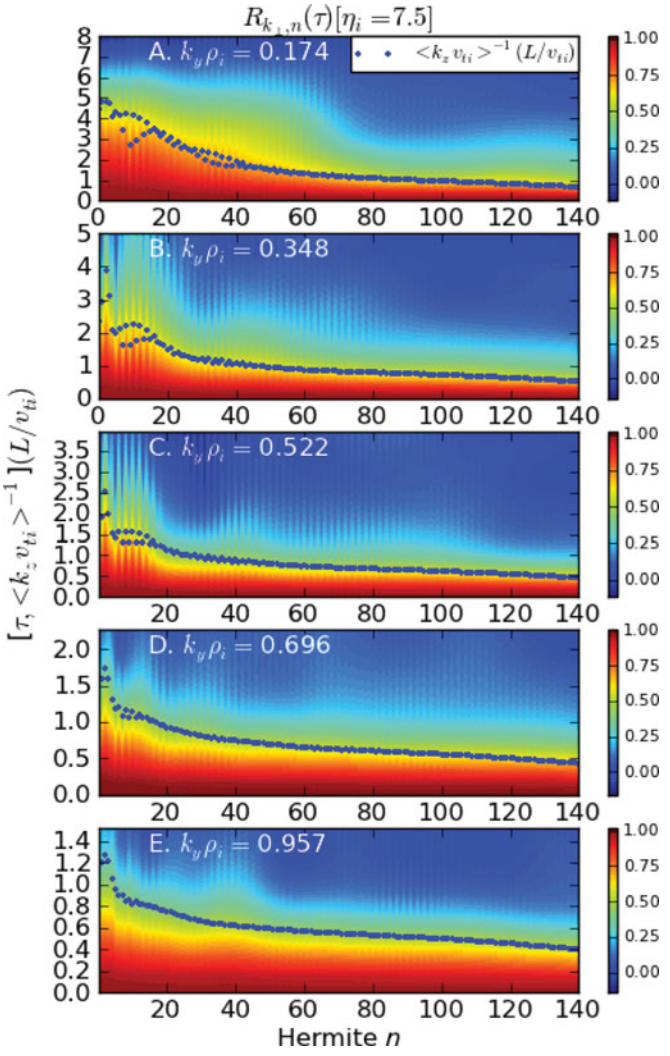

FIGURE 3. (Colour online) Contour plots of the temporal correlation function $R_{k_\perp,n}(\tau)$ for several representative wavenumbers, $k_x = 0$ and $k_y\rho_i = 0.174, 0.348, 0.522, 0.696, 0.957$ for (A)–(E), respectively. Critical balance is manifest in the close correlation between characteristic parallel streaming time $\langle k_z v_{ti}\rangle_n^{-1}$ (dots) and the contours of $R_{k_\perp,n}(\tau)$.

The characteristic parallel wavenumber for the three driving gradients is shown in Fig. 4, where a $\langle k_z\rangle_n \propto n^{1/2}$ scaling is clearly observed for high n (note that the zig-zag in the plot is consistent with the fluctuation in the characteristic velocity shown in Fig. 2). In order to understand the origin of this $\sqrt{n}$ dependence, we consider the nonlinearity corresponding to the k_z-summed distribution function $\hat{f}_{\mathbf{k}_\perp,n} = \sum_{k_z} \hat{f}_{\mathbf{k},n}$ used above to calculate the nonlinear correlation time,

$$\mathcal{N}_{\mathbf{k}_\perp,n} = \sum_{k_z}\sum_{\mathbf{k}'}(k'_x k_y - k_x k'_y)\bar{\phi}_{\mathbf{k}'}\hat{f}_{\mathbf{k}-\mathbf{k}',n} \tag{13}$$

$$\sim (k_x^{(\phi)}k_y^0 - k_x^0 k_y^{(\phi)})\bar{\phi}_{\mathbf{k}^{(\phi)}}\hat{f}_{\mathbf{k}^0-\mathbf{k}^{(\phi)},n}, \tag{14}$$

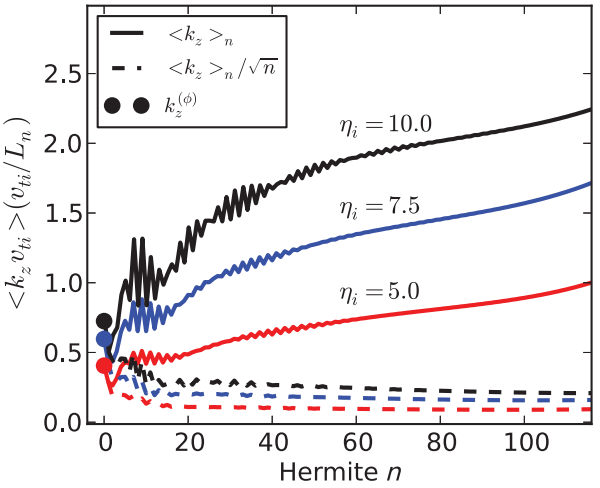

FIGURE 4. (Colour online) The n-resolved characteristic parallel wavenumber $\langle k_z \rangle_n$. The $n^{1/2}$ dependence is highlighted by plotting $\langle k_z \rangle_n / \sqrt{n}$ (dashed lines), which is mostly constant in n at high n.

where (14) is an approximation of (13) arrived at by replacing the sums over wave numbers with a single term representative of the relevant characteristic scale lengths. The sum over $\mathbf{k}'$ is replaced by the contribution from a wave number $\mathbf{k}' = \mathbf{k}^{(\phi)}$ representing the characteristic scale length of the electrostatic potential. Note that the same electrostatic potential enters the nonlinearity for each n. The sum over k_z is approximated by a parallel wave number $k_z^0 = k_z^{(\phi)} + \Delta k_z$ determined in relation to $\mathbf{k}^{(\phi)}$ by the locality of nonlinear interactions. Here Δk_z represents the locality of nonlinear interactions in k_z. Note that the same arguments apply if the sum over $\mathbf{k}'$ is retained as long as Δk_z is only weakly dependent on $k^{(\phi)}$.

Using (14), the nonlinear decorrelation rate is then determined by taking the sum of the characteristic time scales for $\bar{\phi}_{\mathbf{k}^\phi}$ and $\hat{f}_{\mathbf{k}^0 - \mathbf{k}^\phi, n}$. The former is taken by virtue of critical balance for ϕ to be the characteristic parallel wavenumber for the electrostatic potential $\omega_\phi^{\mathbf{k}^{(\phi)}} = k_z^{(\phi)} = \frac{\sum_{\mathbf{k}} |k_z| \varepsilon_{\mathbf{k},0}^{(f)}}{\sum_{\mathbf{k}} \varepsilon_{\mathbf{k},0}^{(f)}}$, and the latter is taken to be the linear phase mixing time scale at Δk_z: $\omega_n^{\mathbf{k}^0 - \mathbf{k}^{(\phi)}} = \sqrt{n}(k_z^0 - k_z^{(\phi)})$. The result is a nonlinear decorrelation rate

$$\omega_{NL}^n \sim k_z^{(\phi)} + \sqrt{n}\left(k_z^{(\phi)} - k_z^0\right) \tag{15}$$

that captures the major features of the n-dependent characteristic parallel wavenumber [note the normalization to v_{ti}/L_n and $1/L_n$ for the frequency and wavenumbers respectively in (15)]. These features can be seen in Fig. 4, where the $\sqrt{n}$ dependence is illustrated with the dashed lines representing $\langle k_z \rangle_n / \sqrt{n} \sim \Delta k_z$, which approach a nearly-constant value at high n. Nonlinear transfer functions verify that the nonlinear energy transfer in k_z is quite local for the $\eta_i = 5.0$ case and becomes progressively less local as η_i increases, consistent with the increasing values of Δk_z identified in Fig. 4.

In summary, the electrostatic potential determines a parallel length scale $k_z^{(\phi)}$ and a time scale $k_z^{(\phi)} v_{ti}$ that are n-independent and present in the nonlinear term for all n. This length scale determines a second length scale $k_z^0 = k_z^{(\phi)} - \Delta k_z$ due to the locality of the nonlinear interactions. The linear phase mixing time scale associated with this locality scale $\sqrt{n}\Delta k_z$ is the source of the $\sqrt{n}$ dependence in the nonlinear correlation time, and by extension via critical balance, in the parallel length scale $\langle k_z \rangle_n$. The

consequences of this n-dependent parallel scale length will be discussed in the next subsection.

4.3. *Hermite free energy spectra*

In order to derive the Hermite free energy spectrum, the $\langle k_z \rangle_n \sim \Delta k_z n^{1/2}$ relation determined above can be directly incorporated into the high-n free energy equation

$$\frac{\partial}{\partial n} n \varepsilon_n = -a_0 n^p \varepsilon_n - S_n, \tag{16}$$

where the first term on the RHS has been generalized so that it can represent either the Lenard Bernstein operator ($a_0 = -\nu/\Delta k_z$ and $p = 1$) or a hypercollision operator ($a_0 = -\nu_h n_{\max}^{-8}/\Delta k_z$ and $p = 8$ for the eighth-order operator used here). The term S_n has been added to represent an additional energy sink. In a full gyrokinetic system this would represent collisional dissipation in perpendicular velocity space – i.e. the dissipation mechanism enhanced by nonlinear phase mixing. In the present system it represents perpendicular hyperdiffusion or, in the context of (10), nonlinear energy transfer to higher $k_\perp$.

Note that the additional factor of $n^{1/2}$ on the LHS of (16) causes the phase mixing term to maintain the same n-scaling as the Hermite free energy spectrum ε_n, i.e. if $\varepsilon_n \propto n^{-\beta}$ has a power law dependence, then the phase mixing term ($\propto \frac{\partial}{\partial n} n^{-\beta+1}$) preserves this same power law. Thus a power law can be maintained even in the presence of an energy sink if the energy sink is proportional to the Hermite free energy spectrum. This is indeed the case for both the perpendicular hyperdiffusion and the nonlinear energy transfer (verified numerically), and the energy sink can be expressed as $S_n = \alpha \varepsilon_n$. See Bratanov et al. 2013 for a mathematically similar example of power law spectra in the presence of dissipation in the context of a modified Kuramoto–Sivashinsky equation.

The energy equation can now be cast in an analytically solvable form $\frac{\partial}{\partial n} n \varepsilon_n = -a_0 n^p \varepsilon_n - \alpha \varepsilon_n$, whose solution is

$$\varepsilon_n = c_0 n^{-1-\alpha} e^{-(n/n_c)^p}, \tag{17}$$

where $n_c = (-a_0/p)^{-1/p}$ denotes the Hermite scale at which the collisional (or hypercollisional) dissipation begins to dominate and the spectrum decays exponentially. The power law spectra predicted by (17) are verified numerically for both the $\alpha = 0$ (i.e. no perpendicular hyperdiffusion) case [Fig. 5(a)] demonstrating $\varepsilon_n \propto n^{-1}$ spectra, and the more physically relevant case $\alpha > 0$ (i.e. including perpendicular hyperdiffusion) for which the spectra are much steeper (the value $\alpha = 0.85$ is determined by a numerical fit).

The Hermite spectrum for the scale range $k_\perp \rho_i < 1$ is shown in Fig. 6, demonstrating that the steep spectrum is maintained in cases where the phase mixing cascade is balanced by nonlinear energy transfer [as modeled by (10)] rather than by the dissipation terms; in Fig. 6, the phase mixing terms (dashed line) are balanced by the nonlinearity (dashed-dotted line), while the dissipation (from the small amount of hyperdiffusion present at $k_\perp \rho_i < 1$) is an order of magnitude smaller.

The full form of (17) is verified in Fig. 7, where the critical Hermite number $n_c = (\nu_h/\Delta k_z)^{-1/8} n_{\max}$ (the value $\Delta k_z = 0.1$ is taken for the $\eta_i = 5.0$ case as determined from Fig. 4) is shown to accurately predict the location at which the spectrum begins to decay exponentially due to hypercollisional dissipation. As can be seen in Fig. 7, n_c provides an excellent estimate of the onset of the dissipation range, and the exponential decay is also closely captured by (17).

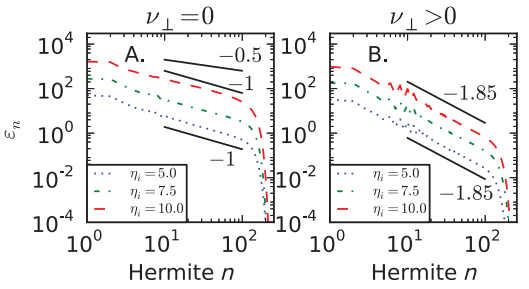

FIGURE 5. (Colour online) Hermite spectra of the free energy ε_n for three different values of the normalized temperature gradient scale length η_i. The spectra are consistent with the power laws defined in (17) for cases with $\nu_\perp = 0$ (A) and $\nu_\perp \neq 0$ (B). Reprinted with permission from D. R. Hatch *et al.*, Phys. Rev. Lett. **111**, 175001 (2013). Copyright 2013 the American Physical Society.

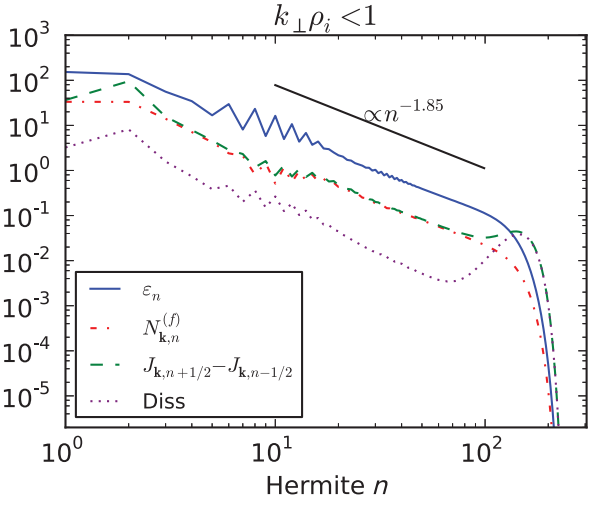

FIGURE 6. (Colour online) Hermite free energy spectrum along with terms in the energy balance equation for the scale range $k_\perp \rho_i < 1$, demonstrating a case where the phase mixing terms (dashed line) are balanced by the nonlinear term (dashed-dotted line), as described in (10).

In Watanabe and Sugama 2004, Hermite spectra approaching n^{-1} are also observed in a model without an additional energy sink (i.e. equivalent to the $\alpha = 0$ case) and using a parallel wavenumber that is tied to k_y. Also in Watanabe and Sugama 2004, the power-laws of the Hermite spectra are observed numerically to depend on collisionality, in contrast with both the analytical expressions derived in (Watanabe and Sugama 2004) and in this work (17). Our numerical observations identify a constant power law for simulations with varying collision frequencies (but otherwise identical parameters) in the inertial range preceding the exponential decay.

At this point it is instructive to consider how the dynamics outlined in this section may be manifest in more comprehensive systems, e.g. full-gyrokinetic toroidal systems or space or astrophysical kinetic turbulence. The steep Hermite spectra are caused by two processes – a nonlinear decorrelation rate that increases with n and the presence of an additional energy sink. Although these processes may not be manifest in exactly the same way in other systems, the trends are expected to be quite general: the strongly

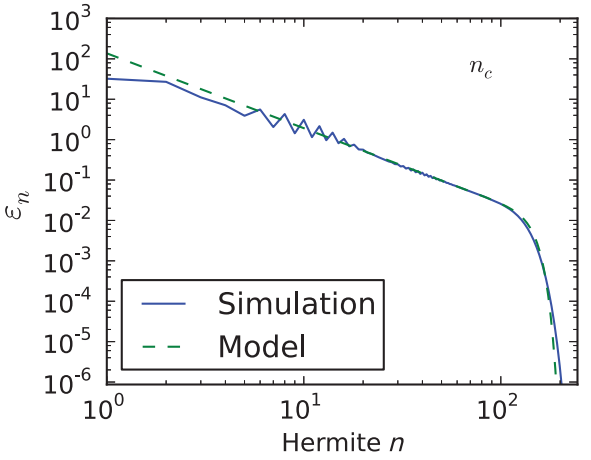

FIGURE 7. (Colour online) Hermite free energy spectrum for the $\nu = 0$ case (only hypercollisions) and $\eta_i = 5.0$ along with the equation defined by (17) using $n_c = (-\nu_h/8\Delta k_z)^{-1/8} n_{\max}$, $\alpha = 0.85$, and $\Delta k_z = 0.1$.

increasing phase mixing time scale $\sqrt{n}k_z$ is expected to enter the nonlinear time scale in some fashion, and an energy sink due to collisions in perpendicular velocity space would be present in any comprehensive system. We thus expect that spectra significantly steeper than the linear $n^{-1/2}$ scaling to be universal in weakly collisional magnetized plasma microturbulence. The consequences of such steep Hermite spectra with respect to dissipation scales are discussed in the next section.

5. Dissipation scales

The Hermite free energy spectra described in the previous section translate directly into Hermite dissipation spectra via the relation $C_n = -2\nu n \varepsilon_n$. For the Hermite spectra, a scaling exponent of negative one is a critical exponent separating collisional dissipation spectra that increase with n from those that decrease with n. As described above, an n^{-1} spectrum can be considered a baseline that is steepened by any additional dissipation due to collisions in perpendicular velocity space or hypderdiffusion. This implies that collisional dissipation in parallel velocity space peaks at large velocity space scales even in arbitrarily low collisionality parameter regimes.

Hermite free energy spectra and resulting collisional dissipation spectra are shown in Fig. 8 for a series of low-collisionality simulations including one using only hypercollisions. The Hermite free energy spectra maintain a (largely) constant power law over the collisionality scan in the n range where collisional dissipation is negligible compared to the phase mixing terms. The end of this 'inertial' range is denoted by the critical Hermite numbers n_c; as seen in Fig. 8, the spectra begin to deviate from a power law shortly preceding these critical Hermite numbers. The (hyper-)collisional dissipation spectra are also shown in Fig. 8; for the collisional cases, the dissipation peaks at the large velocity space scales but spreads farther to smaller scales as the collisionality decreases.

The n dependence of the collisional dissipation is also key to understanding the dissipation scales in the full phase space. Energy is injected at large phase space scales (low k_z and $k_\perp$ in real space, and $n = 2$ in Hermite space), and is thereafter

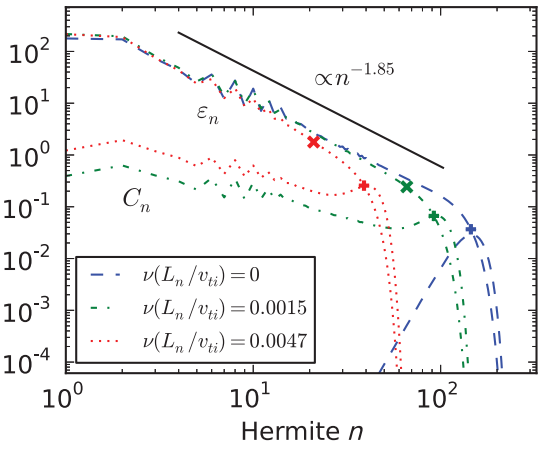

FIGURE 8. (Colour online) Hermite free energy spectra and collisional dissipation spectra (including hypercollisions) for three simulations: $\nu = 0.0047$ (dotted line), $\nu = 0.0015$ (dashed-dotted), and $\nu = 0$ (only hypercollisions) (dashed). The critical Hermite numbers for the collisional dissipation (marked with xs) are $n_c = \Delta k_z/\nu = (21, 67)$ for the two collisional cases, and the critical Hermite numbers for the hypercollisions (marked with + symbols) are $n_c = (\nu_h/8\Delta k_z)^{-1/8} n_{\max} = (40, 92, 145)$ respectively.

subject to energy transfer simultaneously to larger n and $k_\perp$. Since the collisional dissipation peaks at low n and the spectrum decreases with $k_\perp$, this means that energy is transferred to increasingly less-dissipative regions of phase space. As a result, the collisional dissipation will always peak at large scales in phase space. This does not imply, however, that small scales are unimportant; as the collisionality decreases, the dissipation spreads to increasingly smaller scales so that in an integrated sense the small scales can provide the dominant energy sink.

This phase space dependence of the dissipation is illustrated in Fig. 9, which shows the n- and $k_\perp$-resolved (summed over k_z) dissipation from collisions and perpendicular hyperdiffusion for simulations using a broad range of collision frequencies. The dissipation is dominated by $k_\perp$ hyperdiffusion (large scale in n and small scale in $k_\perp$) in the lowest collisionality case (Fig. 9(a)) and transitions to large scale (in $k_\perp$ and n) collisional dissipation as collisionality increases [Figs. 9(b)–(d)]. Note that the strong peaking of the hyperdiffusion in phase space is somewhat deceptive – in the full physical system (including perpendicular velocity space dynamics and a sufficiently large range of small scale wavenumbers $k_\perp \rho_i > 1$), as collisionality decreases, the energy would be distributed and dissipated throughout a progressively larger range of scales (rather than peaking sharply at $k_\perp \rho_i \approx 1.5$ as in Fig. 9).

6. Transition between saturation regimes

The relative importance of large and small scales with respect to dissipation is determined by the competition between the collisional dissipation and the nonlinear energy transfer to $k_\perp \rho_i > 1$; higher collisionality means that more energy is dissipated as it is transferred to higher n and $k_\perp$, whereas faster nonlinear transfer channels energy more quickly to $k_\perp \rho_i > 1$ before it can be dissipated. In (Hatch et al. 2013), the temperature gradient scale length (which determines the growth rate and by extension the saturation amplitude of ϕ and the nonlinear transfer rate) is taken to parameterize the nonlinear transfer rate so that the parameter $L_T/L_C = (\nu L_n/v_{ti})(L_T/L_n)$, where

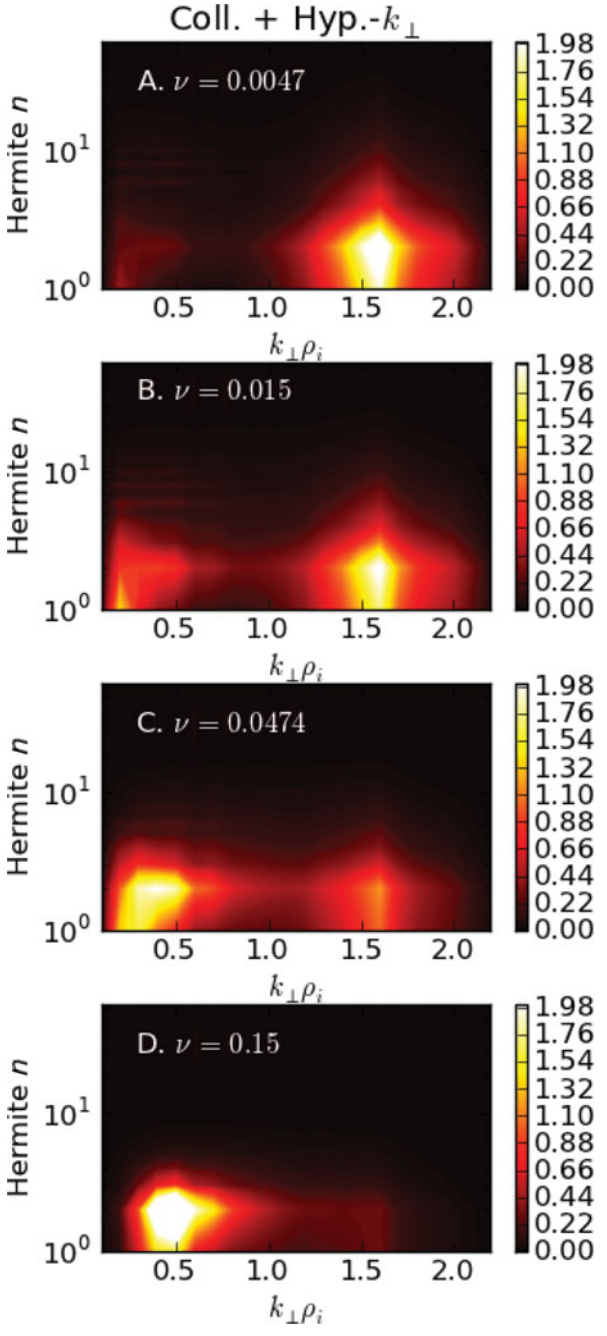

FIGURE 9. (Colour online) Dissipation spectra (including collisions, hypercollisions, and $k_\perp$ hyperdiffusion) in Hermite and $k_\perp$ space (summed over k_z) for a series of simulations with increasing collisionality. As collisionality increases, the dissipation shifts from mostly high-$k_\perp$ (from hyperdiffusion) to mostly low-$k_\perp$ (from collisions).

L_C is the collisional mean free path, is shown to determine a transition between small-scale and large-scale saturation regimes. Here we verify this result with toroidal full gyrokinetic simulations using the GENE code.

We examine a set of high-resolution GENE simulations representing both ITG and electron temperature gradient (ETG) turbulence, scanning ν and R/L_T (R is the major radius), with the remaining parameters centered on the Cyclone Base Case parameter set: normalized density gradient scale length $R/L_n = 2.22$, magnetic shear $\hat{s} = 0.79$ ($\hat{s} = 0.1$ for the ETG cases), safety factor $q_0 = 1.4$, and inverse aspect ratio $\epsilon = 0.18$. The simulations use an s-α equilibrium (with $\alpha = 0$). The GENE collision operator is a comprehensive linearized Landau–Boltzmann collision operator that includes energy and pitch angle scattering as well as conservation terms (Merz 2009; Doerk 2013). We scan collision frequencies ranging from $\nu R/v_{ti} = 0.0086$ to 0.165, and three different temperature gradient scale lengths: $R/L_T = 6.96$ and $R/L_T = 9.5$, which are strongly turbulent, and $R/L_T = 5.0$ which is near-threshold. The electrons (ions) are taken to be adiabatic in the ITG (ETG) case. The definition used for the collision frequency is $\nu_{ss} = e^4 n_{s0} T_{s0}^{-3/2} m_s^{-1/2} \sqrt{2}\pi ln(\Lambda)$, where s denotes the particle species (ions for ITG and electrons for ETG), and $ln(\Lambda)$ is the Coulomb logarithm.

The simulations use $(120, 120, 48, 48, 16)$ grid points in the $(k_x, k_y, z, v_{||}, \mu)$ coordinates, respectively (the perpendicular resolution is increased to 160 for the ETG cases). For the perpendicular wavenumbers this resolution represents the total number of Fourier modes, so that with a box size of $L_x = L_y = 125.6\rho_i$ the simulations resolve up to $k_{\max}\rho_i = 2.95$ (3.95 for the ETG simulations).

In (Hatch et al. 2013), a comparison was made between collisional dissipation in parallel velocity space and perpendicular hyperdiffusion. Here we choose the parameter $D_{k_\perp<1}/D_{k_\perp>1}$ – the ratio of dissipation at large scales ($k_\perp\rho_i < 1.0$) to dissipation at small scales ($k_\perp\rho_i > 1.0$) – as a simple metric for measuring the relative importance of large- and small-scale dissipation. Numerical convergence was established for this parameter at the lowest collisionality $R/L_T = 6.96$ ITG case. As discussed above, linear phase mixing (and the associated collisional dissipation in parallel velocity space) operates at all $k_\perp$ scales, while nonlinear phase mixing (and the associated collisional dissipation in perpendicular velocity space) is negligible at scales larger than the gyroradius. Thus the small-scale contribution $D_{k_\perp>1}$ should be considered an upper bound on the dissipation attributable to collisions in perpendicular velocity space that are facilitated by nonlinear phase mixing. For these GENE simulations the dissipation comes from two sources – collisional dissipation and fourth-order hyperdiffusion in the parallel coordinate. The latter is always a small fraction of the total dissipation and mostly confined to small perpendicular scales. The results for the strongly-turbulent cases are shown in Fig. 10, which shows $D_{k_\perp<1}/D_{k_\perp>1}$ over a range of L_T/L_C along with a subset of the DNA results from (Hatch et al. 2013). In spite of the several differences in the models (the GENE simulations include perpendicular velocity dynamics, toroidal geometry, and sub-gyroscale dynamics), the DNA results and the GENE results show general agreement in the dissipation scales, indicating that the major conclusions drawn from the DNA simulations are likely to hold for a broad range of gradient-driven turbulence scenarios. The GENE results show a higher degree of spread in $D_{k_\perp<1}/D_{k_\perp>1}$ for a given L_T/L_C, which is likely an indication that the temperature gradient scale length is a less accurate indicator of the nonlinear energy transfer rate in the systems studied with GENE simulations.

The near-threshold GENE simulations ($R/L_T = 5.0$) deviate strongly from the other cases, showing a stronger preference for large-scale dissipation for both the ETG and ITG cases, as seen in Fig. 11. This is a result of both linear and nonlinear processes: the maximum linear growth is relatively more strongly decreased in the $R/L_T = 5.0$ case than the other cases [for the gradient scan, the growth rate roughly follows the

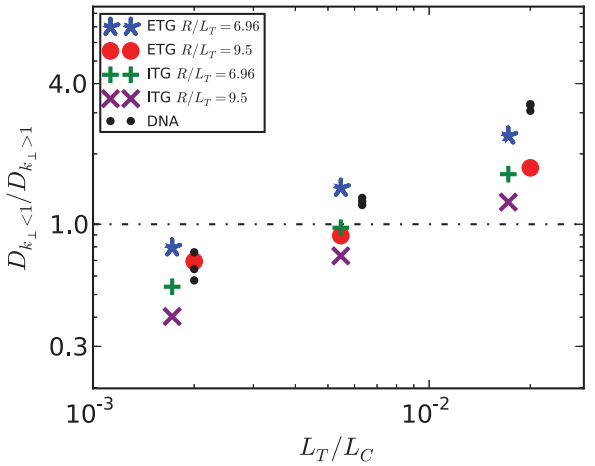

FIGURE 10. (Colour online) The ratio of dissipation at large scales ($D_{k_\perp<1}$) to dissipation at small scales ($D_{k_\perp>1}$) for ITG and ETG simulations scanning collision frequency and temperature gradient scale lengths.

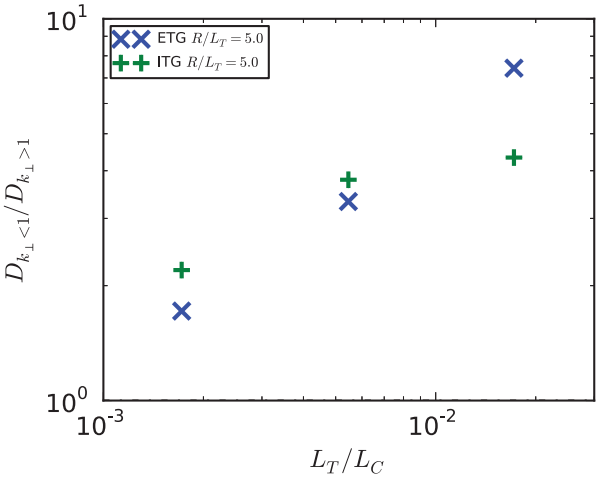

FIGURE 11. (Colour online) The ratio of dissipation at large scales ($D_{k_\perp<1}$) to dissipation at small scales ($D_{k_\perp>1}$) for near-threshold ($R/L_T = 5.0$) ITG and ETG simulations scanning collision frequency. The near-threshold cases exhibit much more large-scale dissipation than the strongly turbulent cases shown in Fig. 10.

relation $\gamma R/v_{ti} \sim 0.1(R/L_T - 4.35)$], and for the ITG simulations the relative zonal flow amplitude is disproportionately amplified in the $R/L_T = 5.0$ case.

In order to put these collisionality scans in the context of present-day fusion devices, we compare the collision frequencies used in the GENE simulations with the experimental ν_* scans described in (Petty 2008). The range of collision frequencies used in the GENE simulations ($\nu R/v_{ti} = 0.0086$–0.165) translates to the range $\nu_* = \frac{e^2 n q_0}{\epsilon^{5/2} T^{3/2} m_i^{1/2}}(a/v_{ti}) = 6.1 \times 10^{-3} - 0.12$, which covers the lower-collisionality portion of Fig. 2 of (Petty 2008). The collisionality scans for some experiments, notably NSTX and Alcator C-Mod, extend to collision frequencies higher than those represented in our scans. It is reasonable to conclude that turbulence in present-day experiments is

characterized by dissipation that is roughly evenly distributed between large and small scales, tending somewhat toward large-scale dissipation scenarios. Near-threshold cases are expected to tend more strongly to large-scale dissipation.

When extrapolating to ITER, two factors should be taken into account. First, collisionality will decrease by approximately an order of magnitude (Petty 2008), and second, the turbulence is expected to tend more toward near-threshold cases, given that the heat flux in gyro-Bohm units will decrease with respect to present-day machines (due, in particular, to the $T^{5.2}$ dependence of the gyro-Bohm heat flux which is only partially compensated by other plasma parameter changes). The former effect will favor small-scale dissipation, while the latter will favor large-scale dissipation. We also note that most space and astrophysical plasmas are substantially less collisional than fusion plasmas, so that nonlinear phase mixing is expected to be a crucial dissipation mechanism in such systems.

7. Summary and discussion

This paper describes a detailed study of the phase space scales of free energy dissipation in gradient-driven gyrokinetic turbulence. The fully spectral DNA code, employing a Hermite representation in parallel velocity space, was used to solve a reduced-gyrokinetic system in conjunction with full gyrokinetic simulations using the GENE code. The Hermite representation used in the reduced model facilitates a detailed study of the energy cascade and resulting dissipation in parallel velocity space scales.

As a first step, the scaling of the Hermite free energy spectrum was examined and found to be much steeper than would be expected linearly. This is due to two factors. First, critical balance was shown to extend to small scales in velocity space (i.e. to high Hermite numbers n). This n-dependent critical balance modifies the energy evolution equation, increasing the Hermite spectrum from $n^{-1/2}$ to n^{-1}. The critically-balanced energy equation, in turn, allows the phase mixing cascade to be balanced by an energy sink that is proportional to the free energy spectrum ($k_\perp$ hyperdiffusion in the present model), further steepening the Hermite spectrum. An expression for the Hermite free energy spectrum was derived and shown to match numerical results in both the power-law inertial range and the exponential decay range.

The consequence of the steep Hermite spectra is that dissipation spectra (scaling like n times the free energy for collisions in $v_{||}$) will always peak at large scales in velocity space. Spectra scaling like $n^{-1.85}$ were observed in the DNA simulations, resulting in strongly decreasing collisional dissipation spectra (scaling like $n\varepsilon_n \propto n^{-0.85}$). Since energy is injected at the $n = 2$ Hermite polynomial, this means that dissipation also peaks at large spatial scales, consistent with earlier studies of gyrokinetic dissipation. Nonetheless small-scale dissipation, like collisional dissipation in perpendicular velocity space due to nonlinear phase mixing, can become dominant in an integrated sense when the collisionality becomes small enough and/or the nonlinear energy transfer becomes large enough.

The relative importance of large-scale and small-scale dissipation was examined in the context of the parameter L_T/L_C, where the temperature gradient scale length R/L_T is taken to roughly parameterize the nonlinear transfer rate. This parameter determines a transition from predominantly small-scale dissipation (at very small L_T/L_C) to predominantly large-scale dissipation as L_T/L_C increases. This transition, originally identified in (Hatch et al. 2013) using the DNA code was verified using

toroidal full-gyrokinetic simulations from the GENE code. The GENE simulations also determined that near-threshold scenarios strongly favor large-scale dissipation.

Ranges of collision frequencies found in present-day experiments correspond to regimes slightly favoring large-scale dissipation (assuming turbulence sufficently distant from threshold). In ITER-like scenarios collision frequencies are much lower (favoring small-scale dissipation), and turbulent regimes more likely to be near-threshold (favoring large-scale dissipation). Low-collisionality space and astrophysical plasma turbulence is expected to strongly favor small-scale dissipation.

From the perspective of fundamental turbulence studies, the value of this work lies in its elucidation of free energy spectra in velocity space and the resulting phase space dependence of dissipation. We do not expect that the Hermite free energy spectra derived here are universal. However, the underlying phenomena are not limited to the gradient-driven systems studied here. The extension of critical balance to high-order moments is expected to be manifest in other low-collisionality, magnetized plasma turbulence scenarios. Likewise, the increasing (with n) nonlinear correlation time and the n-independent energy sink, both of which serve to steepen the Hermite spectrum, are likely manifest in various ways in other scenarios. We thus expect Hermite spectra significantly steeper than the linear $n^{-1/2}$ scaling to be quite universal. Moreover, we conclude that in general, dissipation in gyrokinetic turbulence is fundamentally different than its fluid counterpart: dissipation is not a fundamentally small-scale phenomenon (even in velocity space) – it peaks at large scales in the full phase space and spreads to smaller scales in less-collisional, more nonlinear regimes. As such, there is often little scale separation between drive and dissipation scales, and no $k_\perp$ inertial range in the conventional sense (i.e. a range whose contribution to the total dissipation is negligible).

From a practical standpoint, this work is expected to facilitate and inform reduced modeling efforts, whose goal is to accurately resolve the large-scale low-order moments that determine transport fluxes while modeling small-scale processes with reduced resolution. Examples are Large Eddy Simulation techniques and gyrofluid approaches. Moreover, as the purview of gyrokinetics expands to previously unexplored parameter regimes (e.g. the plasma edge (Jenko et al. 2009; Scott et al. 2010; Wan et al. 2012), ITER, stellarators (Xanthopoulos et al. 2007; Nunami et al. 2012; Helander et al. 2013), and magnetic reconnection (Numata et al. 2011; Pueschel et al. 2011; TenBarge et al. 2014), care must be taken to ensure that dissipation processes are modeled in ways that preserve the accurate resolution of desired quantities. The fundamental understanding of dissipation provided by this work will contribute to a foundation from which such considerations can be rigorously made.

Acknowledgements

Useful conversations with M. Barnes, B. Teaca, P. W. Terry, A. Zocco, N. Loureiro, G. Plunk, and S. Mahajan are gratefully acknowledged. Simulations were performed at the Texas Advanced Computing Center (TACC) at The University of Texas at Austin. Simulations were also carried out using the HELIOS supercomputer system at the International Fusion Energy Research Centre, Aomori, Japan, under the Broader Approach collaboration between Euratom and Japan, implemented by Fusion for Energy and JAEA. The research leading to these results has received funding from the European Research Council under the European Unions Seventh Framework Programme (FP7/2007-2013)/ERC grant agreement no. 277870.

Appendix. Steady state $n \gg 1$ free energy equation

The steady state ($\partial/\partial t \to 0$) energy equation for $n > 2$ is

$$\Re\left[ik_z\pi^{1/2}\left(\sqrt{n}\hat{f}^*_{\mathbf{k},n}\hat{f}_{\mathbf{k},n-1} + \sqrt{n+1}\hat{f}^*_{\mathbf{k},n}\hat{f}_{\mathbf{k},n+1}\right)\right] = N^{(f)}_{\mathbf{k},n} - \nu\pi^{1/2}|\hat{f}_{\mathbf{k},n}|^2. \tag{A1}$$

Using the transformation (Zocco and Schekochihin 2011) $\widetilde{f}_n = (i\,\mathrm{sgn}(k_z))^n \hat{f}_n$, where $\mathrm{sgn}(k_z)$ denotes the sign of k_z, this can be re-expressed as

$$\Re\left[|k_z|\pi^{1/2}\left(-\sqrt{n}\widetilde{f}^*_{\mathbf{k},n}\widetilde{f}_{\mathbf{k},n-1} + \sqrt{n+1}\widetilde{f}^*_{\mathbf{k},n}\widetilde{f}_{\mathbf{k},n+1}\right)\right] = N^{(f)}_{\mathbf{k},n} - \nu\pi^{1/2}|\widetilde{f}_{\mathbf{k},n}|^2. \tag{A2}$$

In the following, we focus on the phase mixing terms [LHS of (A2)], which will be denoted with the notation PM.

The following decomposition is used to separate the amplitude information from the time dependence and phase information:

$$\widetilde{g}_{\mathbf{k},n}(t) = a_{\mathbf{k},n}h_{\mathbf{k},n}(t), \tag{A3}$$

where $a_{\mathbf{k},n} = \frac{1}{T}(\int_{t_1}^{t_1+T}|\widetilde{g}_{\mathbf{k},n}|^2dt)^{1/2}$ and $h_{\mathbf{k},n}(t) = \widetilde{g}_{\mathbf{k},n}(t)/a_{\mathbf{k},n}$. Now using the definitions

$$\begin{aligned}\delta_{\mathbf{k},n+1} &= a_{\mathbf{k},n} - a_{\mathbf{k},n+1},\\ \delta_{\mathbf{k},n-1} &= -a_{\mathbf{k},n} + a_{\mathbf{k},n-1},\end{aligned} \tag{A4}$$

and

$$\sigma_{\mathbf{k},n\pm1} = \Re\left[h^*_{\mathbf{k},n}h_{\mathbf{k},n\pm1}\right], \tag{A5}$$

PM can be rewritten as

$$\begin{aligned}\mathrm{PM} = |k_z|\pi^{1/2}(&-\sigma_{n-1}\sqrt{n}a_n^2 - \sigma_{n-1}\sqrt{n}a_n\delta_{n-1}\\ &+ \sigma_{n+1}\sqrt{n+1}a_{n+1}^2 - \sigma_{n+1}\sqrt{n+1}a_{n+1}\delta_{n+1}),\end{aligned} \tag{A6}$$

which thus far entails only a reformulation of the phase mixing terms in (A1) without any approximations (wave vector subscripts have been suppressed for clarity).

The approximations $\delta_{n\pm1} \to 0$ (approached for $n \gg 1$) and $\sigma_{n\pm1} \to 1$ produce

$$\mathrm{PM} \approx 2|k_z|\left(\sqrt{n+1}\varepsilon_{n+1}^2 - \sqrt{n}\varepsilon_n^2\right), \tag{A7}$$

which is a discretized version of PM in (9).

REFERENCES

Armstrong, T. P., Harding, R. C., Knorr, G. and Montgomery, D. 1970 *Methods in Comput. Phys.* **9**, 29.

Barnes, M., Parra, F. I. and Schekochihin, A. A. 2011 *Phys. Rev. Lett.* **107**, 115003.

Bratanov, V., Jenko, F., Hatch, D. R. and Brunner, S. 2013 *Phys. Plasmas* **20**, 022108.

Bratanov, V., Jenko, F., Hatch, D. R. and Wilczek, M. 2013 *Phys. Rev. Lett.* **111**, 075001.

Cerri, S. S. 2013 private communication.

Doerk, H. 2013 Gyrokinetic simulation of microtearing turbulence. *PhD thesis*, Universität Ulm.

Dorland, W. and Hammett, G. W. 1993 *Phys. Fluids* B **5**, 812.

Doyle, E. J. et al. 2007 *Nucl. Fusion* **47**, S18.

Garbet, X., Idomura, Y., Villard, L. and Watanabe, T. H. 2010 *Nucl. Fusion* **50**, 043002.

Goldreich, P. and Sridhar, S. 1995 *Astrophys. J.* **438**, 763.

Görler, T. and Jenko, F. 2008 *Phys. Plasmas* **15**, 102508.

Grant, F. C. and Feix, M. R. 1967 *Phys. Fluids* **10**, 1356.

Hammett, G. W., Beer, M. A., Dorland, W., Cowley, S. C. and Smith, S. A. 1993 *Plasma Phys. Control. Fusion* **35**, 973.

Hammett, G. W., Dorland, W. and Perkins, F. W. 1992 *Phys. Fluids* B **4**, 2052.
Hatch, D. R., del-Castillo-Negrete, D. and Terry, P. W. 2012 *J. Comp. Phys.* **231**, 4234.
Hatch, D. R., Jenko, F., Navarro, A. B. and Bratanov, V. 2013 *Phys. Rev. Lett.* **111**, 175001.
Howes, G. G. et al. 2006 *Astrophys. J.* **651**, 590.
Howes, G. G. et al. 2011a *Phys. Rev. Lett.* **107**, 035004.
Hatch, D. R. et al. 2011b *Phys. Rev. Lett.* **106**, 115003.
Hatch, D. R. et al. 2011c *Phys. Plasmas* **18**, 055706.
Helander, P., Beidler, C. D., Bird, T. M., Drevlak, M., Feng, Y., Hatzky, R., Jenko, F., Kleiber, R., Proll, J. H. E., Turkin, Y. and Xanthopoulos, P. 2013 *Plasma Phys. Control. Fusion* **54**, 124009.
Jenko, F., Dorland, W., Kotschenreuther, M. and Rogers, B. N. 2000 *Phys. Plasmas* **7**, 1904.
Jenko, F., Told, D., Xanthopoulos, P., Merz, F. and Horton, L. D. 2009 *Phys. Plasmas* **16**, 055901.
Krommes, J. 2012 *Annu. Rev. Fluid Mech.* **44**, 175.
Landau, L. 1946 *J. Phys. USSR* **10**, 25.
Lenard, A. and Bernstein, I. B. 1958 *Phys. Rev.* **112**, 1456.
Loureiro, N. F., Schekochihin, A. A. and Zocco, A. 2013 *Phys. Rev. Lett.* **111**, 025002.
Makwana, K. D., Terry, P. W., Pueschel, M. J. and Hatch, D. R. 2014 *Phys. Rev. Lett.* **112** 095002.
Merz, F. 2009 Gyrokinetic simulation of multimode plasma turbulence, *PhD thesis*, Universität Münster.
Navarro, A. B., Teaca, B., Jenko, F., Hammett, G. W., Happel, T. and the ASDEX Upgrade Team, 2014 *Phys. Plasmas* **21**, 032304
Navarro, A. B. et al. 2011a *Phys. Plasmas* **18**, 092303.
Navarro, A. B. et al. 2011b *Phys. Rev. Lett.* **106**, 055001.
Numata, R., Dorland, W., Howes, G. G., Loureiro, N. F., Rogers, B. N. and Tatsuno, T. 2011 *Phys. Plasmas* **18**, 112106.
Nunami, M., Watanabe, T.-H., Sugama, H. and Tanaka, K. 2012 *Phys. Plasmas* **19**, 042504.
Parker, S. E. et al. 1994 *Phys. Plasmas* **1**, 1461.
Petty, C. C. 2008 *Phys. Plasmas* **15**, 080501.
Plunk, G., Cowley, S. C., Schekochihin, A. and Tatsuno, T. 2010 *J. Fluid Mech.* **664**, 407.
Plunk, G. G. and Tatsuno, T. 2011 *Phys. Rev. Lett.* **106**, 165003.
Plunk, G. G., Tatsuno, T. and Dorland, W. 2012 *New J. Phys.* **14**, 103030.
Pueschel, M. J., Jenko, F., Told, D. and Büchner, J. 2011 *Phys. Plasmas* **18**, 112102.
Schekochihin, A. A., Cowley, S. C., Dorland, W., Hammett, G. W., Howes, G. G., Plunk, G. G., Quataert, E. and Tatsuno, T. 2008 *Plasma Phys. Control. Fusion* **50**, 124024.
Schekochihin, A. A. et al. 2009 *Astrophys. J.* **182**, 310.
Scott, B. D., Kendl, A. and Ribeiro, T. 2010 *Contrib. Plasma Phys.* **50**, 228.
Tatsuno, T. et al. 2009 *Phys. Rev. Lett.* **103**, 015003.
Teaca, B. et al. 2012 *Phys. Rev. Lett.* **109**, 235003.
TenBarge, J. M., Daughton, W., Karimabadi, H., Howes, G. G. and Dorland, W. 2014 *Phys. Plasmas* **21**, 020708.
TenBarge, J. M. and Howes, G. G. 2012 *Phys. Plasmas* **19**, 055901.
Terry, P. W. et al. 2006 *Phys. Plasmas* **13**, 022307.
Wan, W. et al. 2012 *Phys. Rev. Lett.* **109**, 185004.
Watanabe, T.-H. and Sugama, H. 2004 *Phys. Plasmas* **11**, 1476.
Watanabe, T.-H. and Sugama, H. 2006 *Nucl. Fusion* **46**, 24.
Xanthopoulos, P., Merz, F., Görler, T., Jenko, F. 2007 *Phys. Rev. Lett.* **99**, 035002.
Zocco, A. and Schekochihin, A. A. 2011 *Phys. Plasmas* **18**, 102309.